



## **Computational fluid dynamics modeling of mixed convection flows in buildings enclosures**

**Alexander Kayne, Ramesh K. Agarwal**

Department of Mechanical Engineering & Materials Science, Washington University in St. Louis,  
MO 63130, USA.

### **Abstract**

In recent years Computational Fluid Dynamics (CFD) simulations are increasingly used to model the air circulation and temperature environment inside the rooms of residential and office buildings to gain insight into the relative energy consumptions of various HVAC systems for cooling/heating for climate control and thermal comfort. This requires accurate simulation of turbulent flow and heat transfer for various types of ventilation systems using the Reynolds-Averaged Navier-Stokes (RANS) equations of fluid dynamics. Large Eddy Simulation (LES) or Direct Numerical Simulation (DNS) of Navier-Stokes equations is computationally intensive and expensive for simulations of this kind. As a result, vast majority of CFD simulations employ RANS equations in conjunction with a turbulence model. In order to assess the modeling requirements (mesh, numerical algorithm, turbulence model etc.) for accurate simulations, it is critical to validate the calculations against the experimental data. For this purpose, we use three well known benchmark validation cases, one for natural convection in 2D closed vertical cavity, second for forced convection in a 2D rectangular cavity and the third for mixed convection in a 2D square cavity. The simulations are performed on a number of meshes of different density using a number of turbulence models. It is found that k-epsilon two-equation turbulence model with a second-order algorithm on a reasonable mesh gives the best results. This information is then used to determine the modeling requirements (mesh, numerical algorithm, turbulence model etc.) for flows in 3D enclosures with different ventilation systems. In particular two cases are considered for which the experimental data is available. These cases are (1) air flow and heat transfer in a naturally ventilated room and (2) airflow and temperature distribution in an atrium. Good agreement with the experimental data and computations of other investigators is obtained.

**Copyright © 2013 International Energy and Environment Foundation - All rights reserved.**

**Keywords:** Forced, natural and mixed-convection flows; Flows in building enclosures; Natural ventilation; CFD simulations.

### **1. Introduction**

In the past decade, environmental concerns and the rising cost of energy have created a shift in building architecture towards more energy-efficient designs. The primary environmental concern has been the increase in greenhouse gases, due to the increasing fossil fuel consumption for electricity generation and transportation. Since buildings are major consumers of energy for heating, cooling, lighting, etc., an increase in energy efficiency of buildings will contribute towards a significant decrease in emissions. In 2009, buildings were the second-largest energy-consuming sector in the United States (Figure 1), using

up to 33.9% of the nation’s total energy consumption. Buildings also represented 77.8% of the nation’s electrical energy consumption (Figure 2), 44.4% of which is generated through coal combustion (Figure 3). Coal combustion accounted for 34.6% of the nation’s carbon dioxide emissions (Figure 4), and thus for 28.2% of the nation’s overall greenhouse gas emissions (Figure 5). Therefore, to reduce greenhouse gas emissions, there has been an emphasis on increasing the energy efficiency of buildings. Heating, ventilation and air conditioning (HVAC) has become an integral part of all buildings in US and in many parts of the world; the space conditioning now takes up to 53% of the energy consumption by the end user in the residential sector [1]. As a result, there is great deal of emphasis on reducing the HVAC consumption as well as increasing its efficiency.

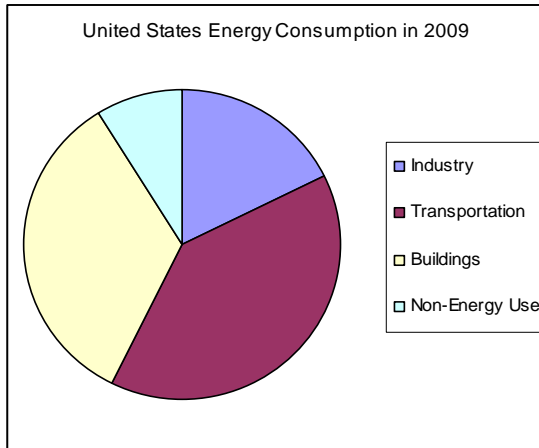


Figure 1. United States total energy usage by sector [2]

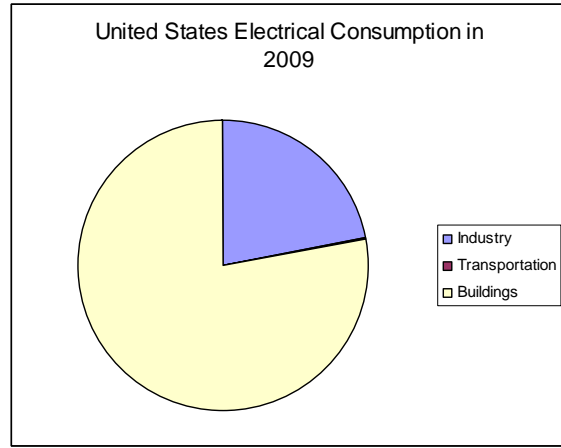


Figure 2. United States electrical energy usage by sector [2]

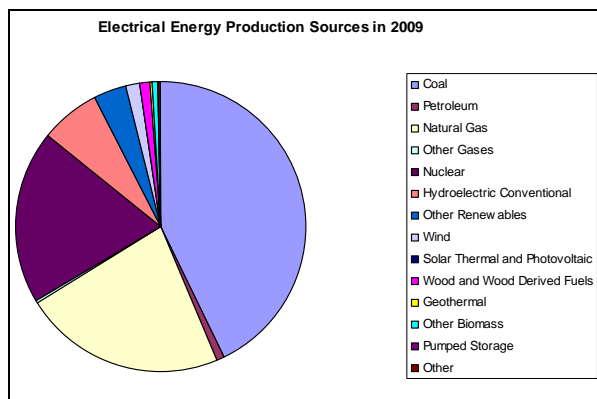


Figure 3. United States electrical energy production sources in 2009 [2]

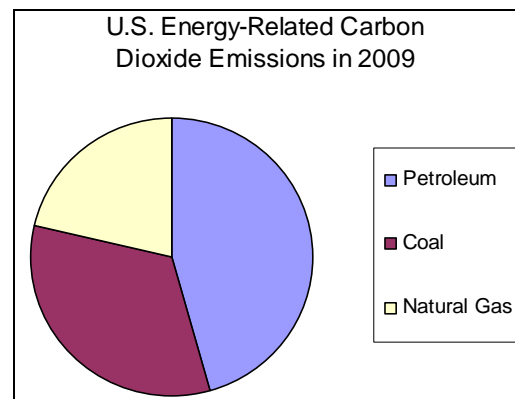


Figure 4. U.S. Energy-related CO<sub>2</sub> emissions in 2009 [3]

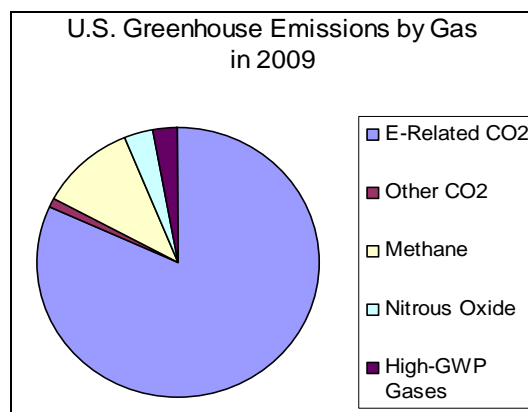


Figure 5. U.S. Greenhouse emissions by gas in 2009 [4]

## 2. HVAC modeling

Due to significant improvements in technology over the past several decades, HVAC is no longer considered a luxury but a basic need in most of the industrialized countries in the world. Considering that the average person in the United States spends over 90% of time indoors [3], coupled with the recognition that goods are “produced better, faster, and more economically in a properly controlled environment” [5], HVAC has become a vital need for both the health of the people and industrial productivity worldwide. Because buildings in different regions of the United States and the world have different heating, cooling and ventilation requirements, it is impossible to create a single energy-efficient and economical HVAC system that can be applied to every building. This can be seen in the balkanization of HVAC industries and materials, in which everything from design to position to setting must be carefully chosen for optimal effect. For the design of energy-efficient HVAC system and to assess and improve the energy efficiency of buildings, building architects and the HVAC industry are increasingly employing flow and heat transfer modeling software to study the flow field in building enclosures as well as to determine the impact of various HVAC systems on thermal comfort.

The main objective of the research reported in this paper is to study the flow field and heat transfer in 3D building enclosures using computational fluid dynamics (CFD) software. For this purpose, the CFD software from ANSYS Inc., called FLUENT 12.1, is employed. The software is first employed to study the flow field in 2-D enclosures for the purpose of code validation and for determining the numerical requirements (mesh, algorithm accuracy, turbulence model etc.) for accurate simulations. Three cases for which experimental data is available are studied. These cases are: (a) a 2-D rectangular cavity with forced convection [6], (b) a 2-D vertical “tall cavity” with natural convection [7], and (c) a 2-D square cavity with mixed convection (combined forced and natural convection) [8]. After code validation with 2-D cases, flow fields in two 3D enclosures are computed. These cases are: (a) a 3-D room with a single heater with natural ventilation [9] and (b) a 3-D atrium with both mixed convection and solar radiation (from a single external glass wall) [10].

In the CFD calculations using FLUENT, we employ the Reynolds-Averaged Navier-Stokes (RANS) equations. Because of the relatively low airspeed in each case, we apply the incompressible form of the equations with the Boussinesq approximation to account for the buoyancy effects. The equations are solved using the second-order upwind SIMPLE algorithm with “PISO” scheme for pressure-velocity coupling. In all the studies, the computations are performed on a sequence of meshes to ascertain that the final solution is mesh-independent. In addition, several turbulence models, in particular the two-equation  $k-\epsilon$  realizable and  $k-\omega$  SST models, are employed to assess the effect of turbulence models on the accuracy of the solutions. The RANS equations and turbulence models (as well as the radiative heat transfer model) create a system of seven equations that are solved numerically which are solved using FLUENT. An analytical solution of these equations is impossible; therefore, an iterative numerical solution method is used on a mesh to approximate the partial differential equations into approximate algebraic equations. The linearized algebraic equations iteratively converge to the nonlinear solutions by employing a suitable algorithm built in FLUENT. A convergence criterion is specified to achieve an acceptable accuracy. When all the flow properties in all cells of the mesh reach the convergence criteria, the solution is considered “converged” and the iterative process ends.

## 3. 2D flow field validation cases

### 3.1 Simulation of forced convection in a 2-D rectangular cavity

The 2-D model employed to study the forced convection in a rectangular cavity was studied experimentally by Restivo [6]. In this model, the rectangular cavity is of height  $H = 3$  m and length  $L = 9$  m. An inlet slot with height  $h = 0.168$  m is made near the upper wall of the cavity, and an outlet slot for air is made near the wall bottom with a height  $t = 0.48$  m as shown in Figure 6. A steady airflow is forced into the cavity chamber at 0.455 m/s, introducing circulation into the cavity. The incoming air has a Reynolds Number of 5000, based on the inlet width, inlet velocity and ambient air conditions. It creates turbulent flow in the chamber. Experiments of Restivo [6] measured the streamwise velocity ( $u$ ) along the vertical axis at  $x = 3$  m and  $x = 2$  m, and along the horizontal axis at  $y = 0.084$  m and  $y = 2.916$  m. Results from our calculations are presented along with the computational results of by Horikiri, Yao and Yao [11] and by De Villiers [12] in Figures 7-12.

In addition to the goal of validation of CFD solver for computing the forced convection flows, one of the key focuses of this test case has been to determine the effect of mesh density and turbulence models on the accuracy of the results. For this purpose, six cases were computed. Computations were performed for

mesh spacing of 0.05 m, 0.01 m and 0.005 m for both k-ε realizable and k-ω SST models. These three meshes resulted in 10800, 270000 and 1080000 nodes.

Figure 7 shows the comparison of our results for three mesh spacing of 0.05 m, 0.01 m, and 0.005 m using the k-ω SST model with the experiments of Restivo [6] and the computations of Horiki, Yao and Yao [11] along the line x = 3 m. Figure 8 shows the comparison of our results for three mesh spacing of 0.05 m, 0.01 m, and 0.005 m using the k-ω SST model with the experimental results of Restivo [6] and the computations of Horikiri, Yao and Yao [11] along the line x = 6 m. From Figures 7 and 8, it can be seen that the agreement between computations and experiment improves between x = 0.7 m and x = 3 m; the discrepancy is larger near the wall between x = 0 m and x = 0.7 m. It can also be noted that the coarser mesh with a spacing of 0.05 m gives poor results.

After determining the appropriate mesh density for accurate simulations, we studied the influence of turbulence models on the accuracy of solutions. Figures 9 and 10 show the computed solutions with both the k-ω SST and k-ε realizable models on a mesh spacing of 0.008 m at x = 3 m and x = 6 m, respectively, and their comparisons with the experimental data of Restivo [6] and the computations of De Villiers [12]. It can be seen from Figures 9 and 10 that the k-ε turbulence model gives a better agreement with the experimental data. Figures 9 and 10 show the velocity profiles along the x-direction at y = 0.084 m and y = 2.916 m, respectively. Although in Figures 9 and 10 none of the models do a good job when compared with the data, the k-ε realizable turbulence model appears to be more accurate compared to the k-ω SST model.

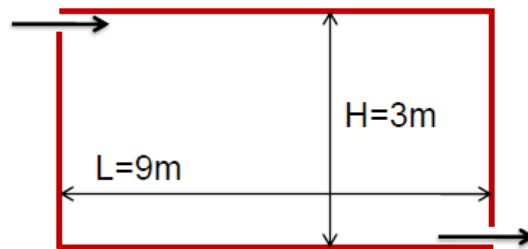


Figure 6. Geometry of the 2-D forced convection model [12]

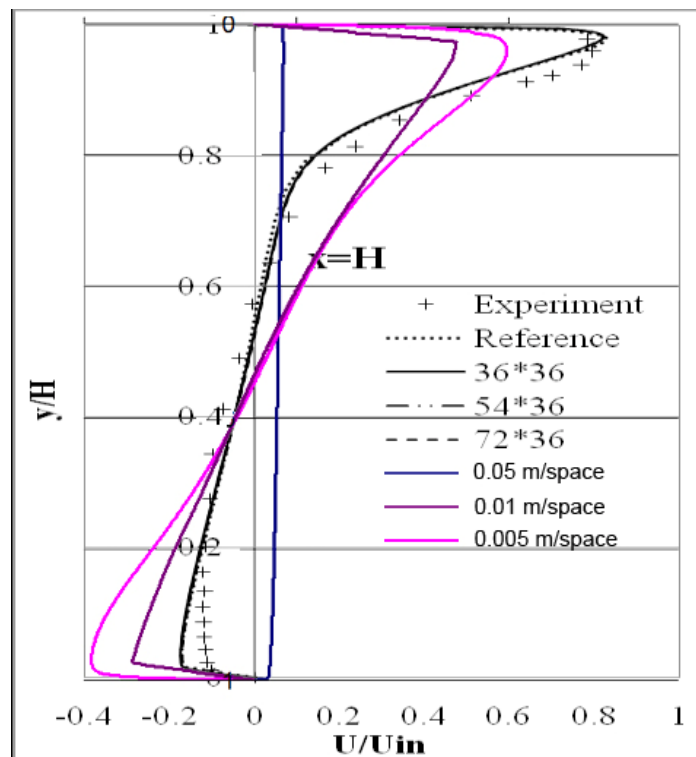


Figure 7. Comparison of present computed results for three different mesh spacing (0.05 m, 0.01 m and 0.005 m) with experimental data of Restivo [6] and the computations of Horikiri, Yao and Yao 2011 [11] at x = 3 m using the k-ω SST turbulence model

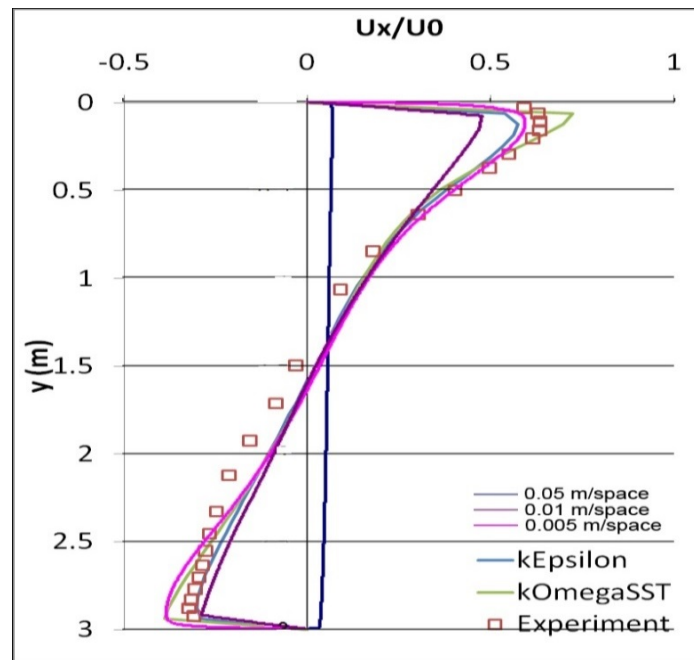


Figure 8. Comparison of present computed results for three different mesh spacing (0.05 m, 0.01 m and 0.005 m) with experimental data of Restivo [6] and the computations of Horikiri, Yao and Yao 2011 [11] at  $x = 6$  m using the  $k-\omega$  SST turbulence model (with  $k$ -Epsilon and  $k$ -Omega SST model)

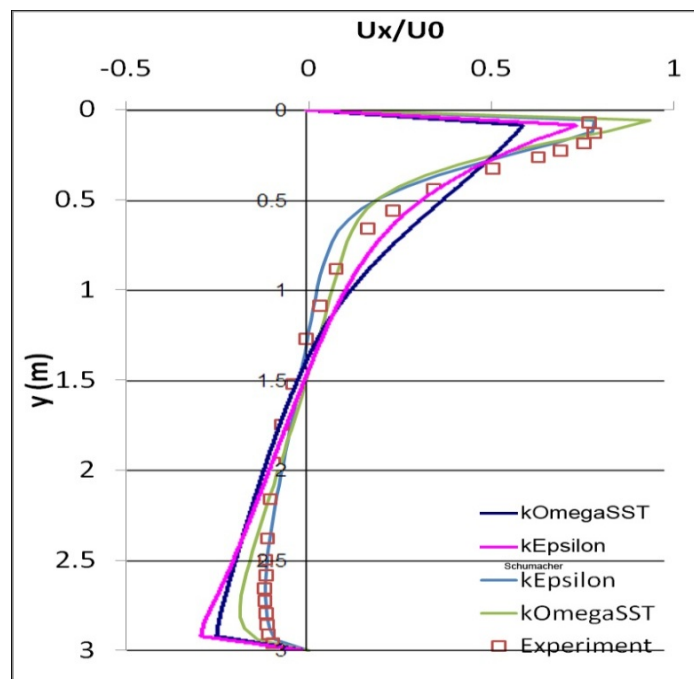


Figure 9. Comparison of present CFD results (in red and dark blue) with the experimental data [6] and computations of de Villiers [12] (in light blue and green) at  $x = 3$  m using the  $k-\epsilon$  Realizable and  $k-\omega$  SST turbulence models

Best results with reasonable computational time are obtained on a mesh of 0.01 m spacing employing the  $k-\epsilon$  realizable turbulence model. Further refinement of mesh spacing to 0.005 m increases the computational time significantly without significant impact on accuracy. Also, the  $k-\omega$  SST turbulence model gives less accurate results when compared to the  $k-\epsilon$  realizable model, especially near the vertical walls of the cavity.

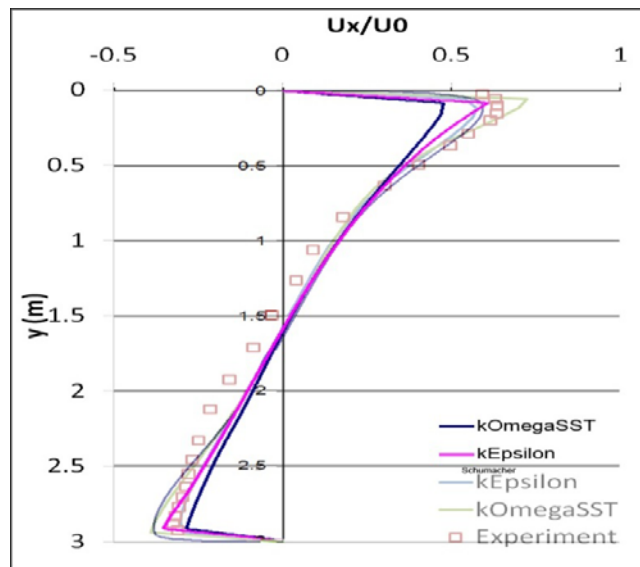


Figure 10. Comparison of present CFD results (in red and dark blue) with the experimental data [6] and computations of de Villiers [12] (in light blue and green) at  $x = 3$  m using the  $k-\epsilon$  Realizable and  $k-\omega$  SST turbulence models

Figures 11 and 12 show the velocity profiles along the x-direction at  $y = 0.084$  m and  $y = 2.916$  m, respectively. Although in Figures 11 and 12 none of the models do a good job when compared with the data, the  $k-\epsilon$  realizable turbulence model appears to be more accurate compared to the  $k-\omega$  SST model. The simulations conducted in this section demonstrate that a suitable mesh spacing and  $k-\epsilon$  realizable turbulence model can model the forced convection flow with acceptable engineering accuracy. It appears that better turbulence models are needed for more accurate prediction.

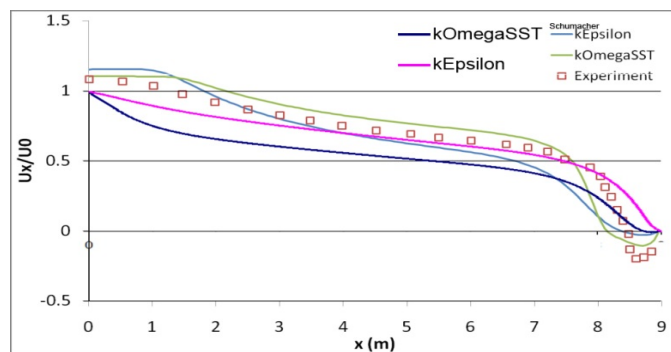


Figure 11. Comparison of CFD Results (in red and dark blue) with experimental data [6] and computations of de Villiers [12] (in light blue and green) at  $y = 0.084$  m using the  $k-\epsilon$  realizable and  $k-\omega$  SST turbulence models

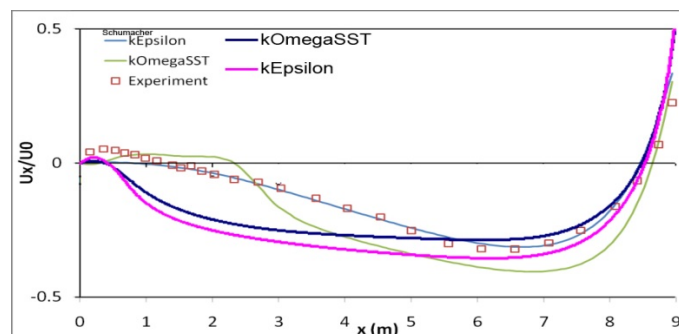


Figure 12. Comparison of CFD Results (in red and dark blue) with experimental data [6] and computations of de Villiers [12] (in light blue and green) at  $y = 2.916$  m using the  $k-\epsilon$  realizable and  $k-\omega$  SST turbulence models

### 3.2 Simulation of natural convection in a 2-D vertical rectangular cavity

This model is based on an experimental study performed by Betts and Bokhari [7]. The model in their experiment (Figure 13) is a tall, hollow closed cavity with no inlets or outlets. The cavity has height  $H=2.18$  m, width  $W=0.076$  m, and depth  $D=0.52$  m. The vertical walls (closest to one another) are polished aluminum plates, one heated to 288.25 K and the other at 307.85 K. The top and bottom walls are assumed to be adiabatic. These flow conditions correspond to a Rayleigh Number ( $Ra$ ) of  $8.6 \times 10^5$ , defined as:

$$Ra = \frac{g\beta(T_h - T_t)H^3}{\nu\alpha} \quad (1)$$

where  $\bar{T}$  is the air temperature at the center of the cavity. Although the experiment was performed in 3-D, the enclosure in Figure 13 can be modeled as nominally 2-D. Having established in section 3.1 that nearly 150000 to 700000 mesh points are sufficient to obtain reasonably accurate results, a mesh spacing of 0.001 m was employed in this case for acceptable accuracy without excessively increasing the computational time. The key goal of this study was to determine the relative accuracy of the two turbulence models for natural convection flow. Present computations are compared with the experimental data of Betts and Bokhari [7] and the computations of Zuo and Chen [13] and de Villiers [12].

Figures 14-19 show the comparison of present computations with the experimental data of Betts and Bokhari [7] and with the computations of Zuo and Chen [13] and of de Villiers [12] at various locations in the cavity for both the velocity and temperature profiles. Unlike the forced convection case in section 3.1, in this case the  $k-\omega$  SST model gives more accurate results. While the realizable  $k-\epsilon$  realizable model gives a reasonable prediction of temperature and velocity profiles in the de Villiers [12] study, the  $k-\omega$  SST model employed in the present study gives results in closer agreement with the experimental data, especially in capturing the velocity peaks at various  $x$ -locations. It also gives more accurate results for the velocity and temperature in the  $y$ -direction ( $y/H = 0.05$ ,  $y/H = 0.1$ ,  $y/H = 0.9$ , and  $y/H = 0.95$ ), thus supporting the claim in the literature that the  $k-\omega$  SST turbulence model is superior in modeling the near-wall layers [14]. This case provides an excellent validation of the CFD solver for computing natural convection flows.

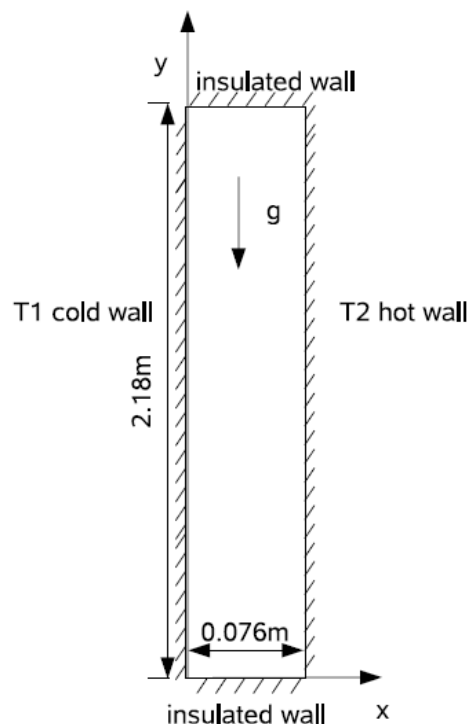


Figure 13. Geometry of the 2-D vertical cavity for natural convection flow simulation [13]

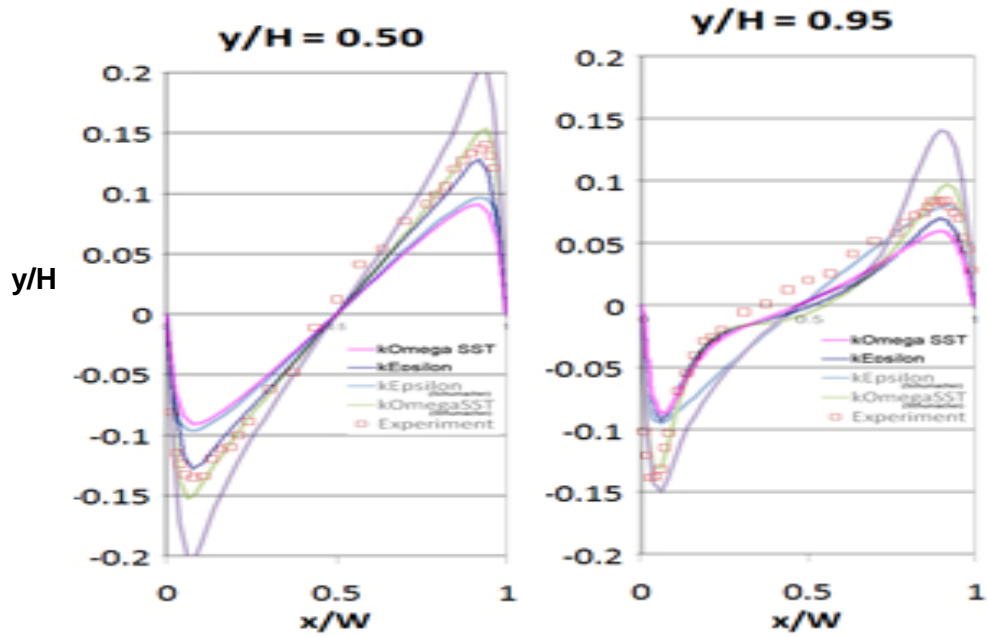


Figure 14. Comparisons of present computations for vertical velocity profiles using the  $k-\omega$  SST and  $k-\epsilon$  realizable turbulence models (in red and dark blue) with experimental data [7] and the computations of de Villiers [12] (in green and light blue)

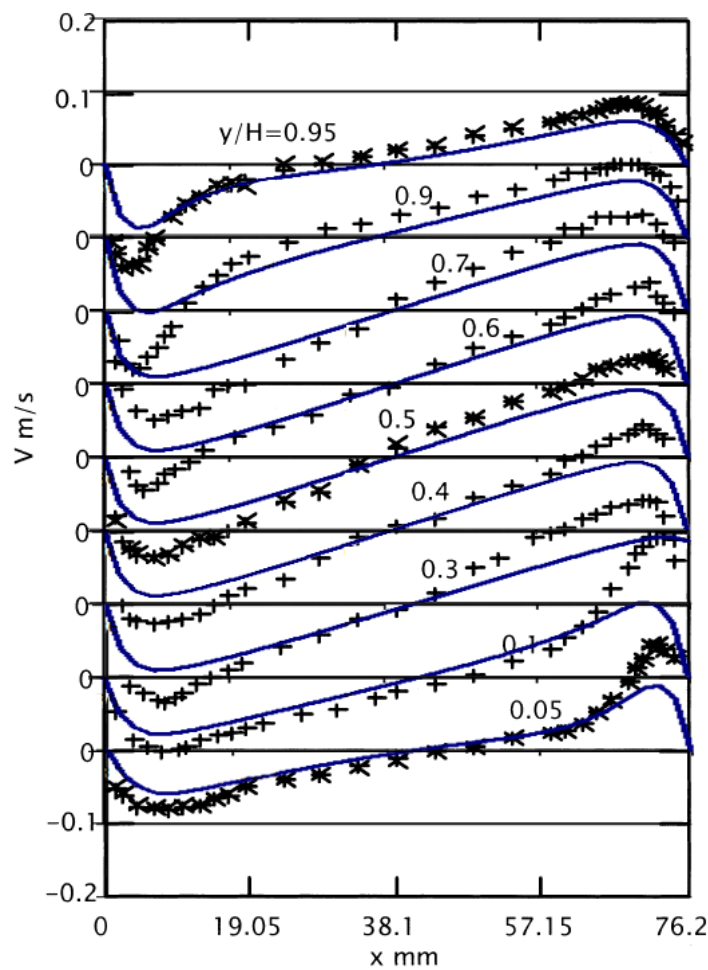


Figure 15. Comparisons of present computations for vertical velocity profiles at various  $y/H$  using the  $k-\epsilon$  realizable turbulence model with experimental data [7]

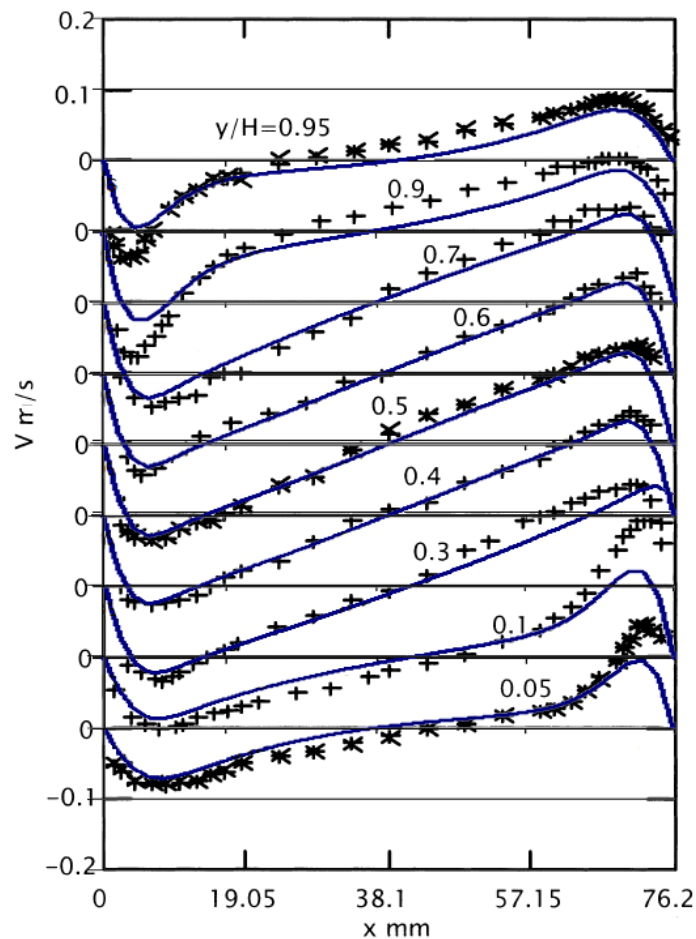


Figure 16. Comparisons of present computations for vertical velocity profiles at various  $y/H$  using the  $k-\omega$  SST turbulence model with experimental data [7]

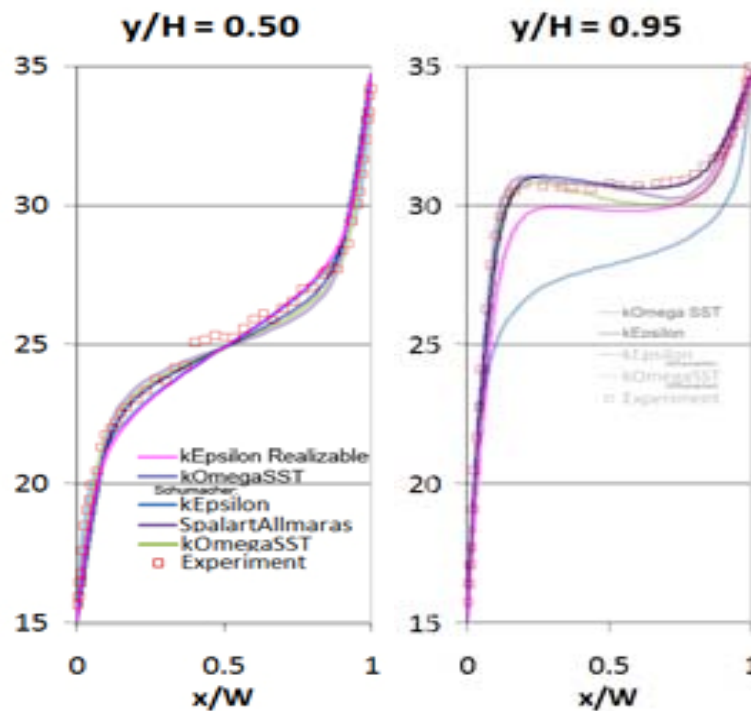


Figure 17. Comparison of present computations for temperature profiles using the  $k-\omega$  SST and  $k-\epsilon$  realizable turbulence models (in light blue and red) with experimental data of [7] and the computations of de Villiers [12] (in green and light blue)

### 3.3 Simulation of mixed convection in a 2-D square cavity

This case is based on the experimental study of Blay et al [8]. In this case (Figure 20), air is forced into a 1.04 m square cavity through an inlet of length  $h_{in} = 0.018$  m on the chamber's ceiling. Like the forced convection case of section 3.1, the air creates circulation within the chamber, and comes out through an outlet of length  $h_{out} = 0.024$  m near the floor. Also, like the natural convection case of section 3.2, the walls ceiling and floor are kept at different temperatures. The temperature of the sides, walls and ceiling is fixed at  $T_{wl} = 288.15$  K, while the floor is kept at  $T_{wh} = 308.65$  K. As a result, the air in the cavity is subjected to both a mixture of inertial and buoyancy forces. This case therefore represents mixed convection.

The key goal of this study is again to validate the CFD solver for computing mixed convection flow, and to determine the relative accuracy of k- $\epsilon$  realizable and k- $\omega$  SST models. Figures 21 and 22 respectively show the vertical temperature profile in the middle of the cavity and the horizontal temperature profile in the middle of the cavity. In this case, present computations with the k- $\epsilon$  realizable model are in closer agreement with the experimental data, although the k- $\omega$  SST model also gives acceptable results. The computational results of de Villiers [12] show a greater disagreement with the experimental data.

Figures 23 and 24 respectively show the comparison of experimental velocity contours (shown by arrows) with those computed by Zuo and Chen [13] using the k- $\epsilon$  realizable and k- $\omega$  SST turbulence models. It can be seen that the flow field velocity contours computed with the k- $\omega$  SST model are in better agreement with the experimental data.

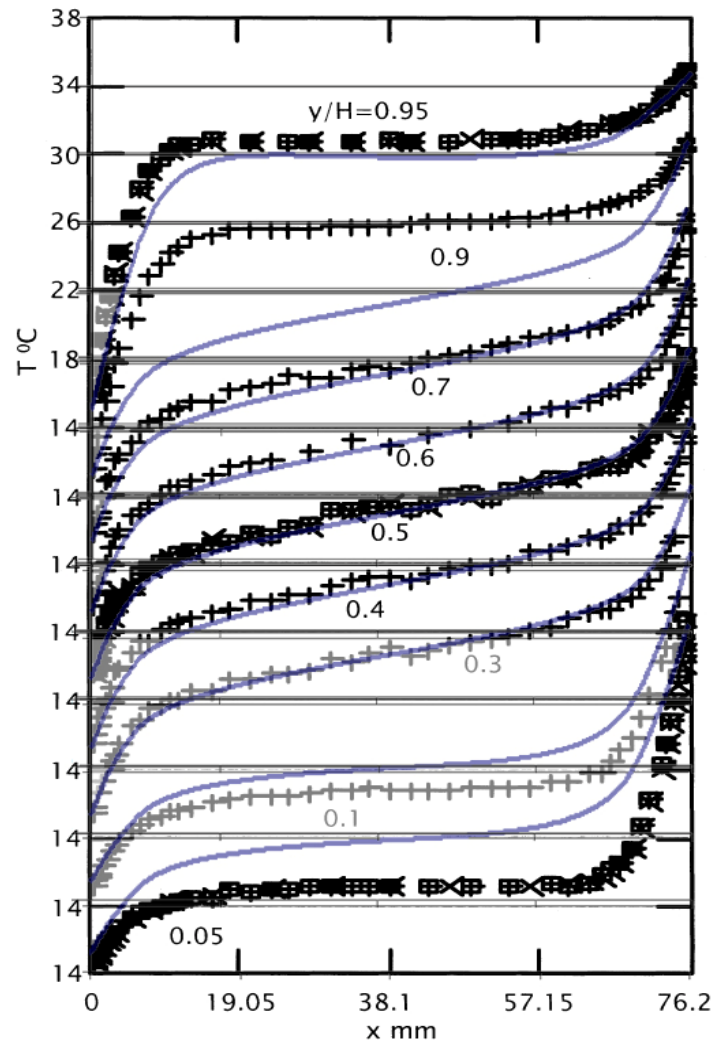


Figure 18. Comparison of present computations for temperature profiles at various  $y/H$  with the experiments [7] using the k- $\epsilon$  realizable turbulence model

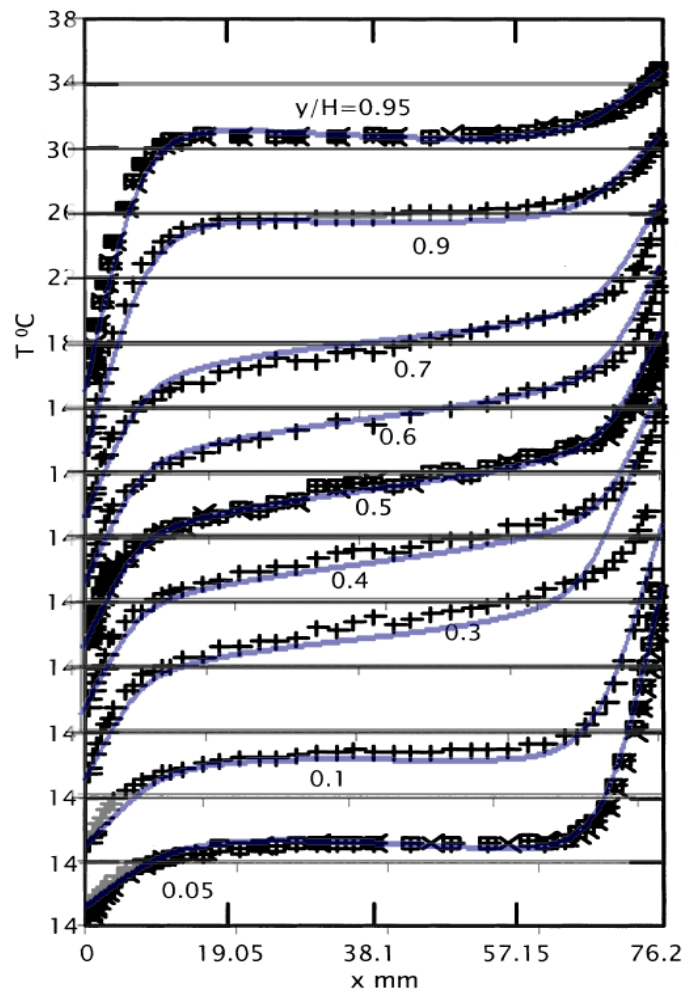


Figure 19. Comparison of present computations for temperature profiles at various  $y/H$  with the experiments [7] using the  $k-\omega$  SST turbulence model

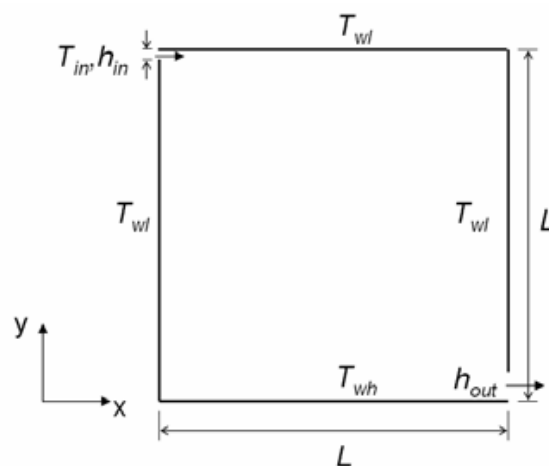


Figure 20. Geometry of the mixed convection model [13]

#### 4. 3D simulation in enclosures

##### 4.1 Modeling air flow in a 3-D enclosure in natural ventilation

This model is based on the experimental study of Jiang and Chen [9] to simulate the indoor environment of a 3-D chamber with a single outlet. In the study, a  $5.16 \times 3.57 \times 2.18 \text{ m}^3$  room was supplied with a single 1,500 W baseboard heater to generate buoyancy forces. In addition, a  $0.9 \times 1.80 \text{ m}^2$  opening was constructed in the opposite wall to simulate fluid flow between the room and a “windless” outdoor

environment, thereby creating single-sided ventilation driven by buoyancy forces. Figure 25 shows the two views describing the floor plan of the room.

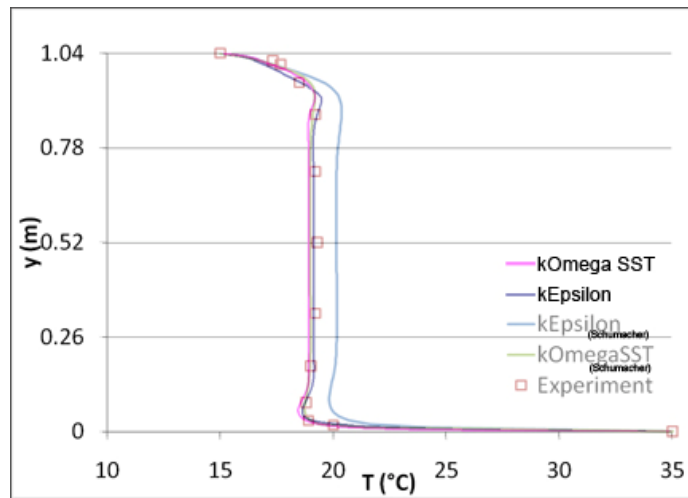


Figure 21. Comparison of present computations for the temperature profile at  $x = L/2$  using the  $k-\epsilon$  realizable and  $k-\omega$  SST turbulence models (in dark blue and red) with experimental data [8] and the computations of de Villiers [12] (in light blue and green)

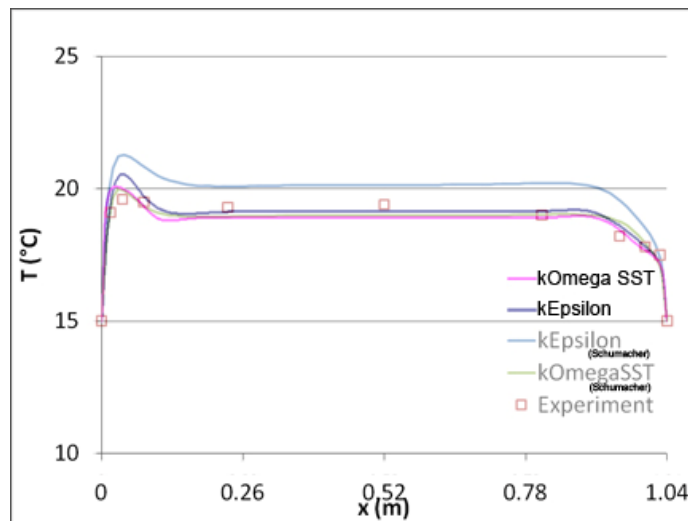


Figure 22. Comparison of present computations for the temperature profile at  $y = L/2$  using the  $k-\epsilon$  realizable and  $k-\omega$  SST turbulence models (in dark blue and red) with experimental data [8] and the computations of de Villiers [12] (in light blue and green)

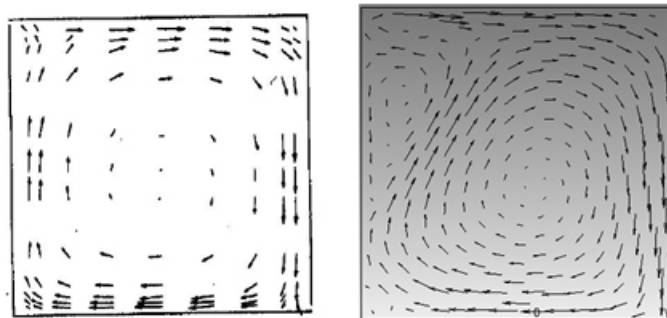


Figure 23. Comparison of experimental velocity contours (left) [13] with present computed velocity contours (right) using the  $k-\epsilon$  realizable turbulence model

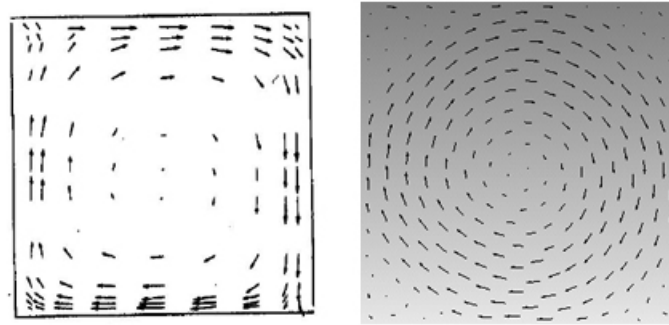


Figure 24. Comparison of experimental velocity contours (left) [13] with present computed velocity contours (right) using the  $k-\omega$  SST turbulence model

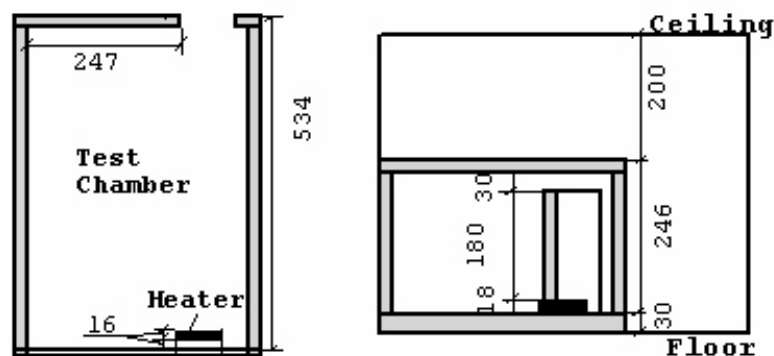


Figure 25. Floor Plan of the room in the 3-D natural convection experiment [9] (all dimensions in cm's)

In this study, air velocity and temperature distributions were measured with six hot-sphere anemometers at different heights (0.1 m, 0.5 m, 0.9 m, 1.3 m, 1.7 m, and 2.1 m from the floor) in five different locations (Jiang and Chan [9]) as shown in Figure 26. These devices displayed considerable uncertainty at air velocities of less than 0.1 m/s; temperature measurement error was 3 K. In addition, since the goal of the study was “to examine the overall airflow pattern in a room scale driven by buoyancy forces” (Jiang and Chan [9]), the heater's surface temperature and micro-scale thermal environment was not measured. Figure 27 shows the 3-D geometry of the room used in the computational study.

In the absence of the availability of detailed data from the experiment, several assumptions were made in the computations regarding the wall, heater and air temperatures. While the heater was modeled with the same dimensions (0.16 m x 0.74 m x 0.18 m) as stated in the experimental study, the temperature along all five exposed walls was assumed to be 350 K. The surrounding walls were assumed to be adiabatic, held at 300 K, and the air characteristics were assumed to be the same as those given in section 3 for the 2-D cases. The window was assumed to be a pressure outlet with a gauge pressure of 0; the air outside the enclosure was assumed to be at 288 K. Based on our good experience with the  $k-\omega$  SST model in the 2-D natural convection problem described in section 3, this turbulence model was chosen for this study.

Figure 28 shows the computed temperature contours in the room's section that contains temperature probes P2, P3 and P5. As can be seen from the contours, the solution satisfies the adiabatic wall conditions in the room with the exception of the window outlet through which air flows through freely. The contours also show that aside from the air immediately surrounding the heater, temperature remains between 288 and 300 K. Figures 29 and 30 are the velocity vector plots in the same section that contains the P2, P3 and P5 probes. Both Figures 29 and 30 show qualitatively similar results inside the chamber; however, there is significant difference in the flow field near the ceiling. In both figures the air enters through the lower section of the window, moves rapidly near the floor and the wall, and circulates back along the ceiling to exit the room on the upper section of the outlet. The computation shows evidence of recirculation in the upper left corner of the room; however, unlike the Jiang and Chan [9] results, the airstream diverges into two distinct areas: one continues the recirculation pattern and the other moves at higher speed straight towards the ceiling. The reason for this behavior is currently under investigation.

Figures 31 and 32 respectively show the comparisons of experimental [9] and computed temperature and velocity profiles at four of the five probe locations. The fifth probe, being outside of the room, has been

neglected. Since the computational model was created based on a number of assumptions due to paucity of information, a direct comparison with the experimental data is not possible; therefore, a qualitative analysis is given. The experimental temperature profiles show close resemblance with their numerical counterparts. Specifically, temperatures remain low near the floor and increase with height. Velocity profiles also show similar results, indicating an area of stagnation near the center of the room which is surrounded by the circulating air. Qualitatively, the experimental and computational results show similar trends in velocity and temperature profiles.

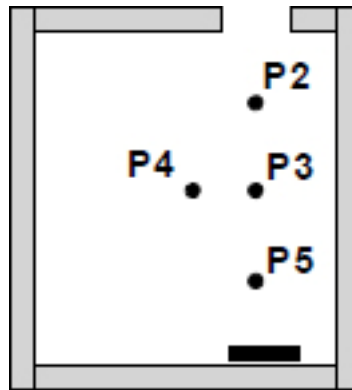


Figure 26. Location of temperature and velocity probe positions in the vertical cross-section [9]

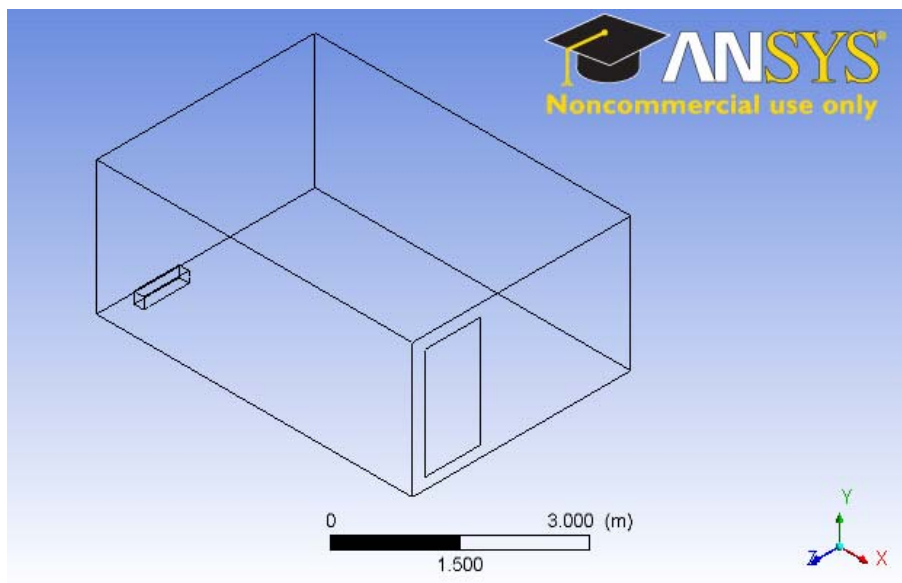


Figure 27. Geometry of the 3-D natural convection model

#### 4.2 Modeling of air flow in a 3-D atrium under forced convection and solar radiation

This test case is based on the experiments performed by Basarir [10] in the atrium of Concordia University's engineering building (Figures 33-35). The atrium's size is 12.05 m x 9.39 m x 13.02 m, and it contains both a supply and return vent on its east wall. The supply vent forces air at a temperature of 288 K into the room at a speed of 4.5 m/s; the Reynolds number is 146,633 based on the floor conditions at the supply vent. The Reynolds number indicates that the flow is turbulent.

The atrium's main feature is an argon-filled double-glazed glass façade that covers the entire south wall. This glass façade has a transmittance of 36%, an absorptivity of 17.5%, and a thermal conductivity of 0.0626 W/m-K and thickness of 24 mm. Noting variables such as wind speed and clear weather, the effective sky temperature was calculated to be 14.21° C, and the solar direction vector was calculated to be (-0.60, 0.69, -0.40) at the time of the experiment [10].

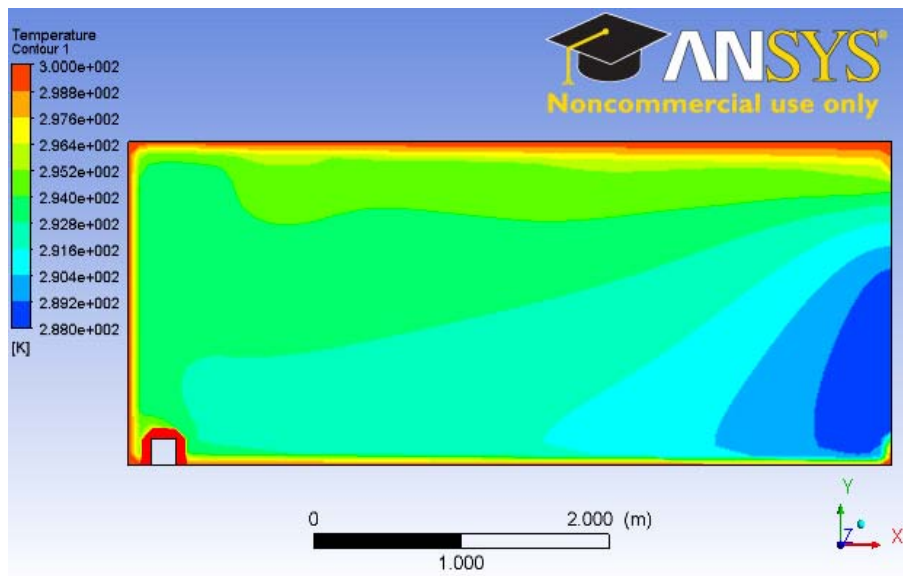


Figure 28. Computed temperature contours in the 3D room at a section containing probes P2-P3-P5

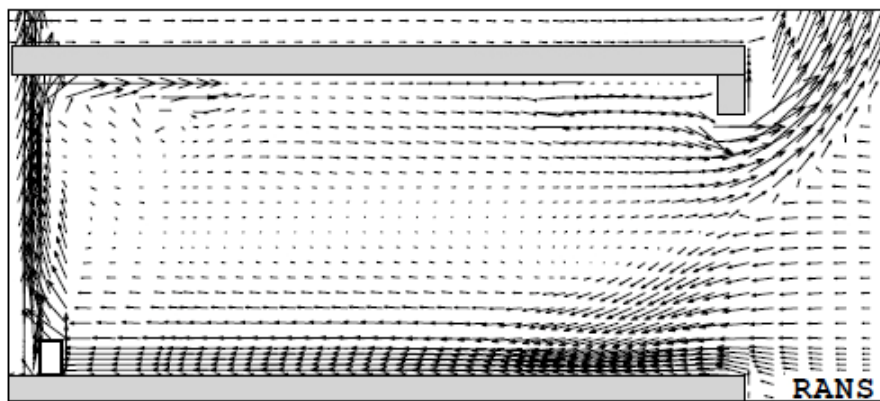


Figure 29. Experimental velocity vector contours inside the section containing the P2, P3, and P5 Probes [9]

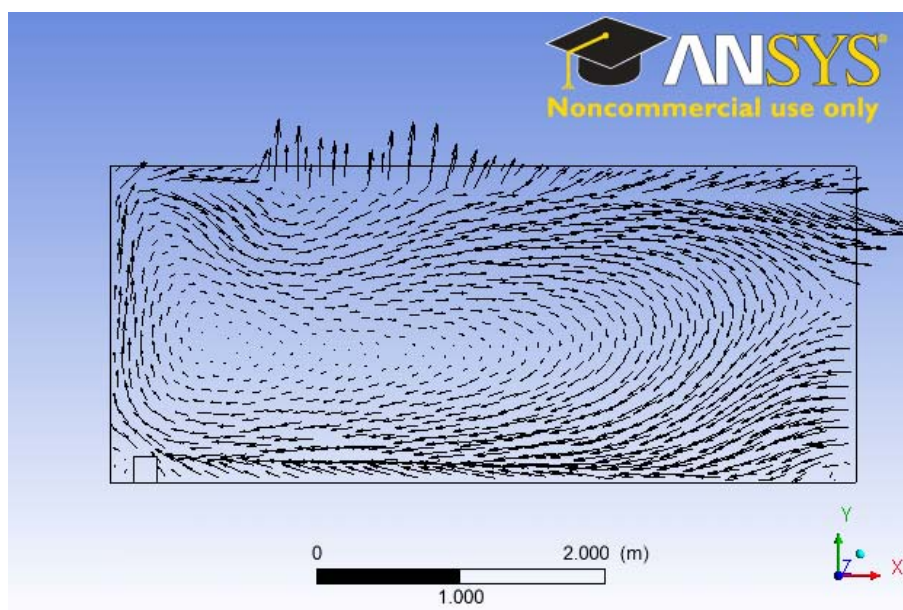


Figure 30. Computed velocity vector contours using the k- $\omega$  SST Model inside the section of the room containing the P2, P3, P5 Probes

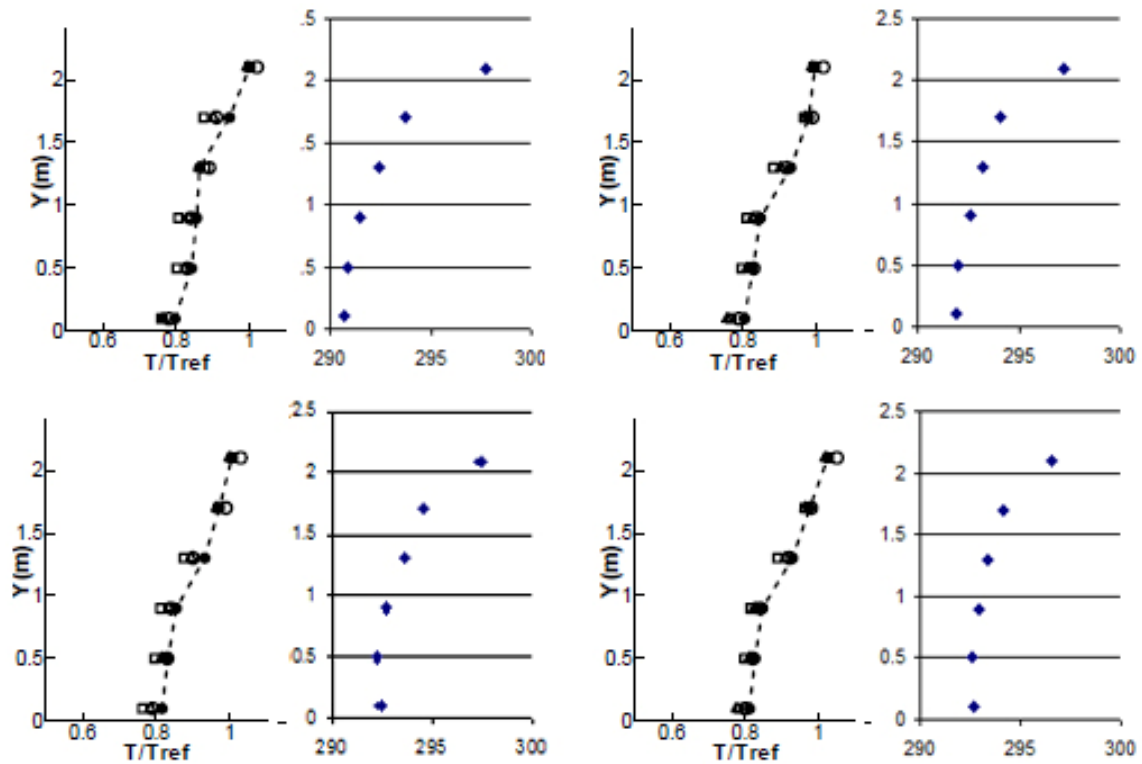


Figure 31. Comparison of experimental (left) [9] and computed (right) results for mean air temperature profiles at P2, P3, P4, and P5 locations

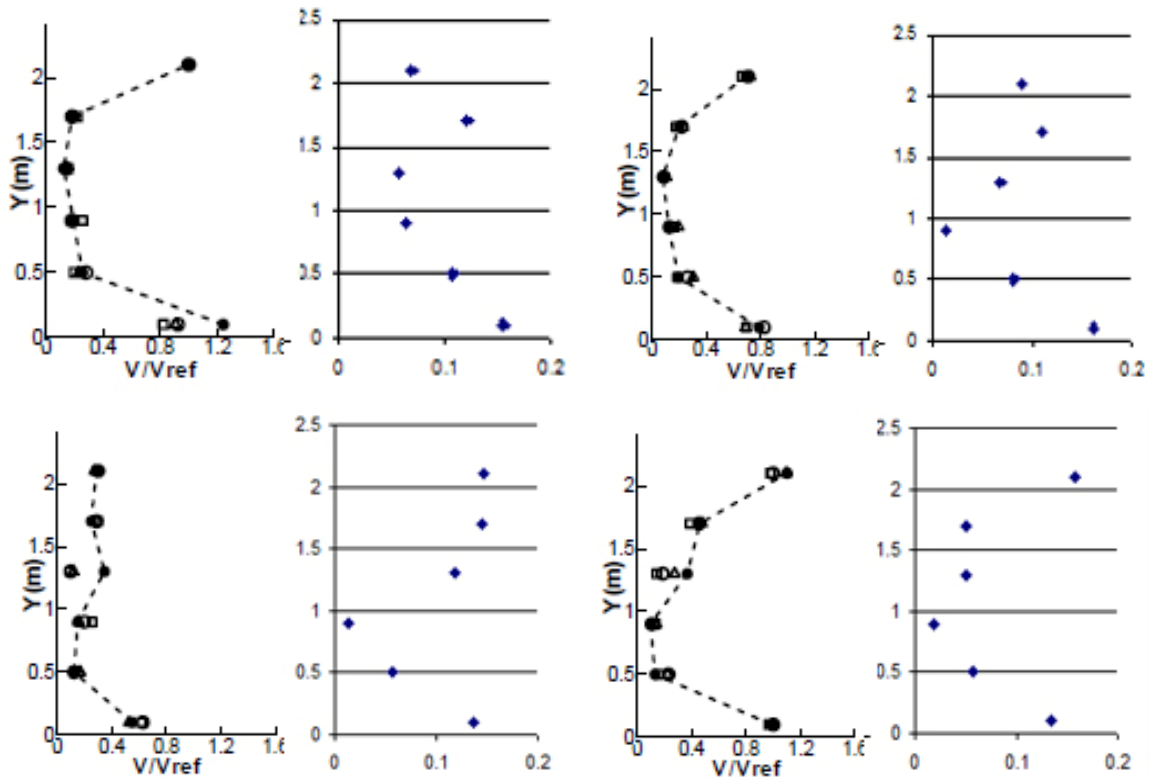


Figure 32. Comparison of experimental (left) [9] and computed (right) results for mean air velocity profiles at P2, P3, P4, and P5 locations

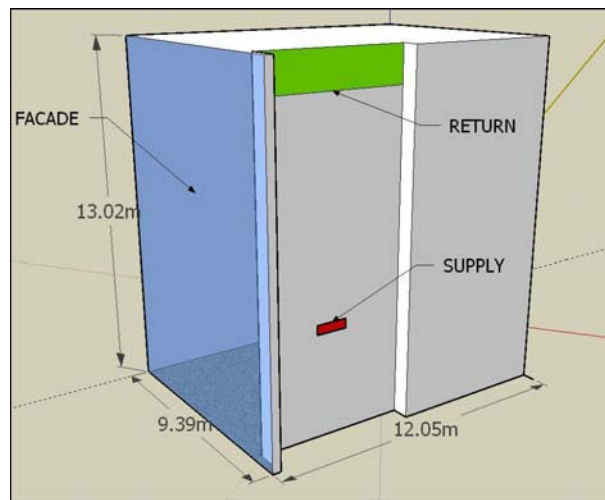


Figure 33. Atrium of Concordia University's Engineering Building [10]

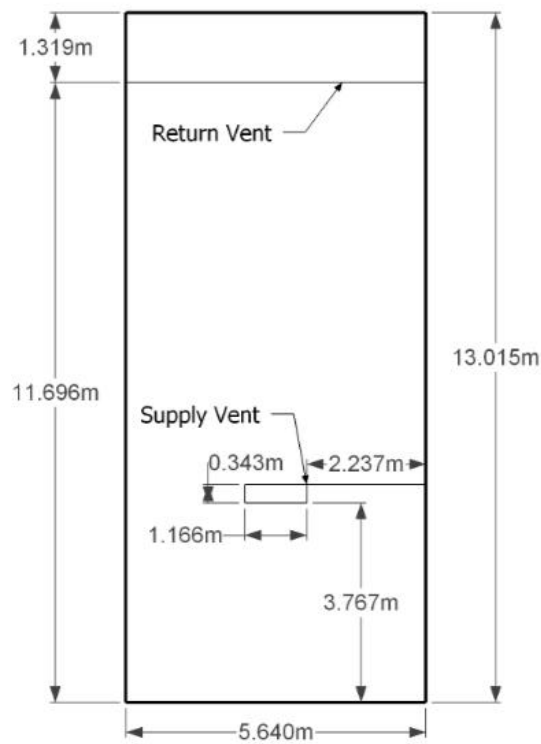


Figure 34. Dimensions of the supply and return vents on the east wall of the Atrium [10]

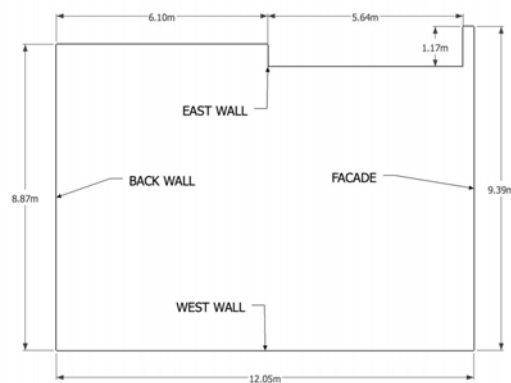


Figure 35. Floor plan of the Atrium [10]

Our goal is to create a CFD model that could reproduce the experimental results; in particular, the temperature profile of the building at 4:00 PM on August 1, 2007 [10]. The mesh inside the atrium model was constructed using a mesh size of 0.125 m. This generated a mesh with 844584 nodes, necessitating a computationally intensive simulation. To reduce the computational time, the convergence criteria were reduced to  $1 \times 10^{-4}$ . The k- $\epsilon$  realizable turbulence model was chosen for this case since it had proven to be more accurate in both the 2-D forced- and mixed Convection cases described in section 3. The Discrete Transfer Radiation (DTR) model was activated in FLUENT to track the effects due to solar radiation. It is important to note here that the glass façade cannot be opaque because it transmits the solar radiation inside the atrium. Therefore its material properties should be carefully taken into account in the CFD model.

Figures 36 and 37 respectively show the temperature contours on the building's façade from the Basarir's [10] experimental study and the present computational study using the k- $\epsilon$  model. It can be noted from both the figures that the left side of the façade is considerably warmer than the rest of the façade. This means that the left side of the atrium will be warmer than the rest of the atrium due to "a wall that partially traps the hot air." Furthermore, the lower right side has a considerable accumulation of cold air near the right wall, possibly due to the "impingement of the cool supply air on this wall." There is also evidence of circulation in both the figures, particularly in the lower middle part of the room. It should be noted, however, that on the whole, the computational results computed with the k- $\epsilon$  model show lower temperatures than in Basarir's experiments.

Figures 38 and 39 respectively show the contour plots of the numerically predicted temperatures by Basarir [10] and by the authors of this paper at heights of 2, 6.165 and 10.25 meters above the floor. Once again it can be noticed that there is a considerable accumulation of cold air on the lower end of the west wall, and the effects of the trapped air on the east end of the façade have become more pronounced. Especially noteworthy are the low-temperature contours running parallel to the façade in the  $y = 2$  plane. These contour plots, and the fact that they are below the supply vent, lend credence to Basarir's claim that the circulation is responsible for the cool air against the east wall. Again, our computed temperature distribution obtained with the k- $\epsilon$  realizable model is cooler than that obtained by Basarir [10].

Experimental data for this study was collected via a network of 12 thermocouples on the glass façade and 21 additional thermocouples distributed in the interior space of the atrium. As a result, it is possible to compare experimental data with numerical results in greater detail as shown in Tables 1 and 2. As can be seen from these tables, the k- $\epsilon$  model yields very accurate results for the façade, particularly on the upper level of the building where deviation from experimental results is  $\sim -0.5\%$ . The same could not be said of the air temperature results, as they are consistently 12-15% lower than the experimental data.

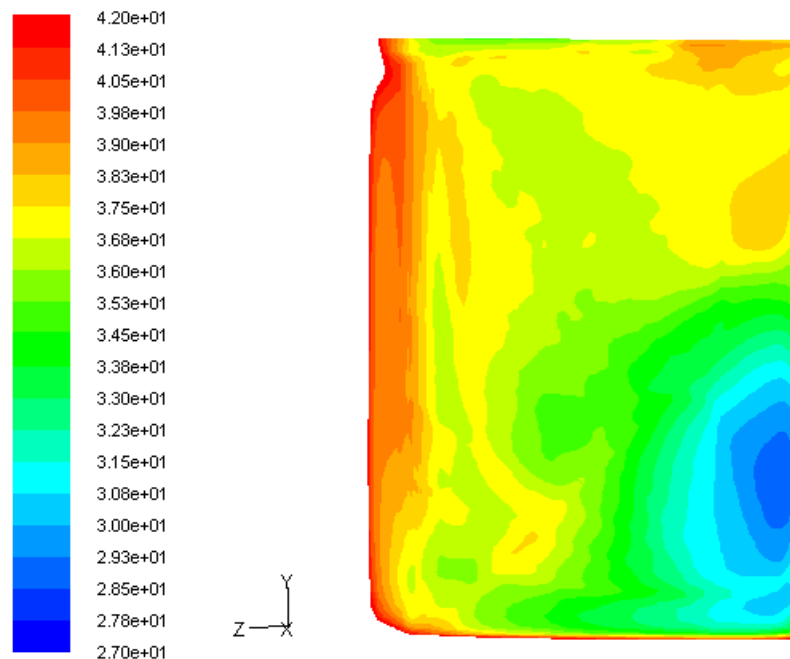


Figure 36. Temperature contours in  $^{\circ}\text{C}$  on the glass façade in Basarir's Experiment [10]

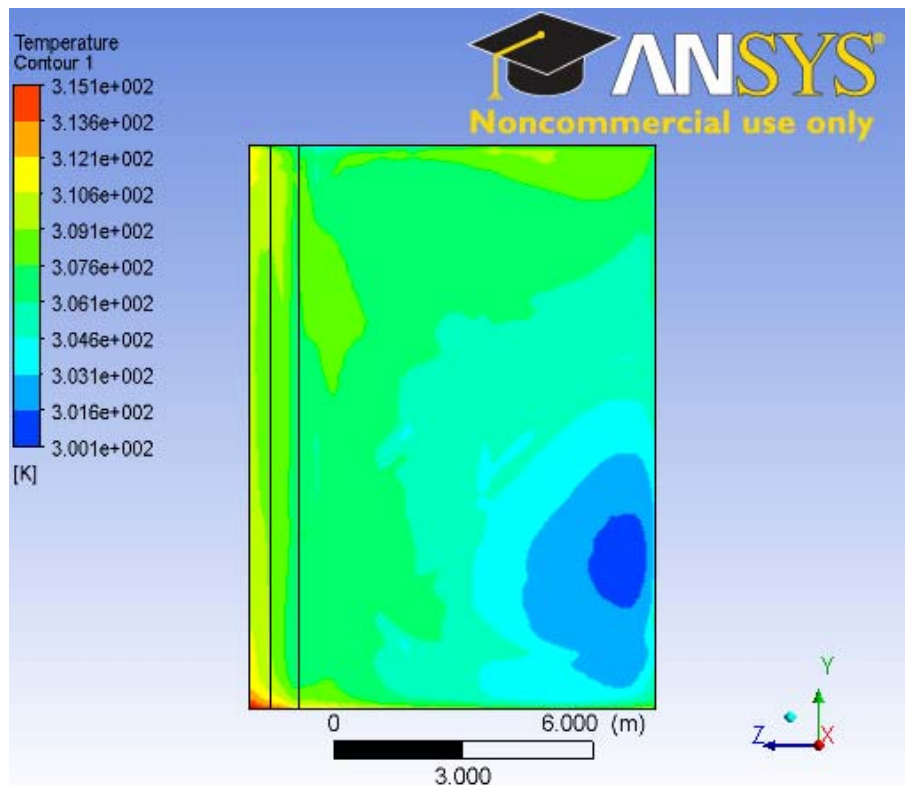


Figure 37. Computed temperature contours in °K on the glass façade using the k- $\epsilon$  realizable turbulence model

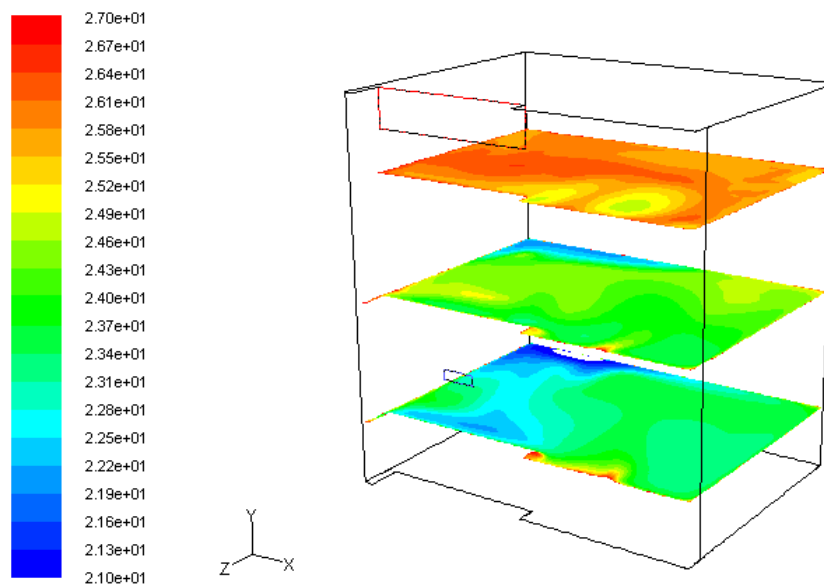


Figure 38. Temperature contours in °C in the Atrium in  $y = 2$ ,  $y = 6.165$  and  $y = 10.25$  planes in Basarir's computations [10]

It can be noticed from Table 2 that temperatures in the experiment and simulations are in close agreement. In particular, the temperatures remain low near the floor and increase with height. Velocities show similar trends, indicating a period of stagnation near the center of the room which is surrounded by the circulating air.

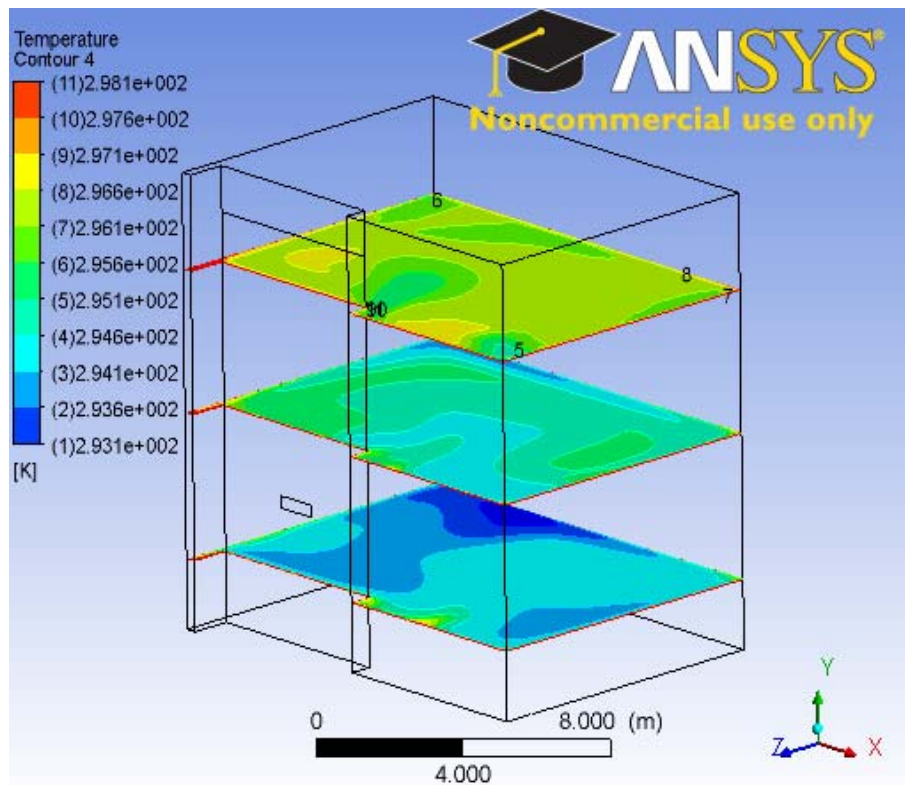


Figure 39. Temperature contours in °K in the Atrium at  $y = 2$ ,  $y = 6.165$  and  $y = 10.25$  planes in the present computations using the  $k-\epsilon$  realizable turbulence model

Table 1. Temperatures on the glass façade: Comparison between experimental data [10] and present computations (coordinates indicate to thermocouple locations)

GLASS HIGH	Coordinates	Temperature T (°C)		$\Delta T$ (°C)	Percent Difference
		Exp.	Num.		
FL_G_T	0,10.25,7.26	34.20	34.66	0.46	1.3%
FM_G_TH	0,10.9,4.22	34.90	33.80	-1.10	-3.2%
FM_G_TL	0.9.35,4.22	33.60	33.47	-0.13	-0.4%
FR_G_T	1,10.25,1.24	32.80	32.93	0.13	0.4%
Average		33.88	33.72	-0.16	-0.5%
GLASS MID	Coordinates	Temperature T (°C)		$\Delta T$ (°C)	Percent Difference
		Exp.	Num.		
FL_G_M	0,6.165,7.26	31.70	34.19	2.49	7.8%
FM_G_MH	0,6.9,4.22	34.10	32.00	-2.10	-6.1%
FM_G_ML	0,5.2,4.22	31.70	31.56	-0.14	-0.5%
FR_G_M	0,6.165,1.24	32.50	30.45	-2.05	-6.3%
Average		32.50	32.05	-0.45	-1.4%
GLASS LOW	Coordinates	Temperature T (°C)		$\Delta T$ (°C)	Percent Difference
		Exp.	Num.		
FL_G_B	0,2.1,7.26	30.90	33.33	2.43	7.9%
FM_G_BH	0,3.05,4.22	30.10	31.41	1.31	4.3%
FM_G_BL	0,1.35,4.22	29.50	32.63	3.13	10.6%
FR_G_B	0,2.1,1.24	29.80	28.76	-1.04	-3.5%
Average		30.08	31.53	1.46	4.9%

Table 2. Air temperatures: Comparison between experimental data [10] and present computations (coordinates indicate to thermocouple locations)

AIR HIGH	Coordinates	Temperature T (°C)		$\Delta T$ (°C)	Percent Difference
		Exp.	Num.		
FL_R_T	0.24,10.25,7.26	26.80	23.55	-3.25	-12.1%
FM_R_TH	0.24,10.9,4.22	28.20	23.44	-4.76	-16.9%
FM_R_TL	0.24,9.35,4.22	27.20	22.86	-4.34	-15.9%
FR_R_T	0.24,10.25,1.24	26.60	24.00	-2.60	-9.8%
EW_16	5.96,10.25,7	26.20	22.24	-3.96	-15.1%
WW_16	5.78,10.25,1.05	26.10	22.98	-3.12	-11.9%
AA_16	8.81,10.25,4.44	26.30	23.26	-3.04	-11.6%
Average		26.77	23.19	-3.58	-13.4%

AIR MID	Coordinates	Temperature T (°C)		$\Delta T$ (°C)	Percent Difference
		Exp.	Num.		
FL_R_M	0.24,6.165,7.26	25.90	22.52	-3.38	-13.1%
FM_R_MH	0.24,6.9,4.22	25.60	21.68	-3.92	-15.3%
FM_R_ML	0.24,5.2,4.22	24.40	21.69	-2.71	-11.1%
FR_R_M	0.24,6.165,1.24	26.30	21.00	-5.30	-20.1%
EW_15	5.96,6.165,7	24.50	21.39	-3.11	-12.7%
WW_15	5.78,6.165,1.05	25.10	21.72	-3.38	-13.5%
AA_15	8.81,6.165,4.44	24.60	21.61	-2.99	-12.2%
Average		25.20	21.66	-3.54	-14.1%

AIR LOW	Coordinates	Temperature T (°C)		$\Delta T$ (°C)	Percent Difference
		Exp.	Num.		
FL_R_B	0.24,2.1,7.26	23.90	21.70	-2.20	-9.2%
FM_R_BH	0.24,3.05,4.22	23.90	21.49	-2.41	-10.1%
FM_R_BL	0.24,3.05,4.22	23.40	21.10	-2.30	-9.8%
FR_R_B	0.24,2.1,1.24	23.00	20.53	-2.47	-10.7%
EW_14	5.96,2.1,7	24.00	20.90	-3.10	-12.9%
WW_14	5.78,2.1,1.05	22.30	20.77	-1.53	-6.8%
AA_14	8.81,2.1,4.44	23.00	21.13	-1.87	-8.1%
Average		23.36	21.09	-2.27	-9.7%

## 5. Conclusions

The goal of the work presented in this paper has been to assess the modeling requirements and accuracy of CFD computations using RANS equations for forced-, free-, and mixed- convection flows in 3-D building enclosures. The CFD simulation software FLUENT 12.1 is employed for this purpose. In order to determine the modeling requirements and accuracy of the RANS simulations, the experimental test data is used for validation of computation.

The 2-D simulation cases served as the validation cases for the CFD software and provided guidelines about the mesh size and turbulence models that should be employed for obtaining solutions of acceptable engineering accuracy.

A 3-D room with natural ventilation was modeled; this configuration corresponds to the experimental model studied by Jiang and Chen [9]. The computations for velocity and temperature profiles in various regions of the room showed reasonable agreement with the experimental data. Detailed quantitative comparisons could not be obtained because of lack of detailed information about the flow conditions and other parameters from the experiment (e.g. the information about the surface heater temperature). Nevertheless, the CFD simulations were satisfactory. As another example, the 3D flow field inside an atrium was computed; the experimental data for the atrium was obtained from Basarir [10]. This flow in the atrium represents a mixed convection flow with solar radiation. Good comparison between the computation and experiment was obtained for the velocity and temperatures inside the atrium. The

maximum discrepancy between the computations and experiments was 10-15%, depending on the region inside the atrium. In many parts of the atrium, the agreement between computation and experiment was excellent, within 0.5% of each other. It is surmised that a finer mesh will improve the accuracy of CFD predictions in regions where there is greater discrepancy.

In summary, it is demonstrated in this paper that CFD can model the flow field and heat transfer in building enclosures quite accurately with a proper choice of mesh density and the turbulence model.

## References

- [1] Pérez-Lombard, L., Ortiz J., and Pout, C., 2008, "A Review on Buildings Energy Consumption Information," *J. of Energy and Buildings*, Vol. 40, pp. 394-398.
- [2] International Energy Agency, 2011, "Energy Balances of OECD Countries."
- [3] U.S. Environmental Protection Agency, 1995, "The inside Story: A Guide to Indoor Air Quality," Washington D.C., accessed by Web. on 4 Apr 2012, <<http://www.epa.gov/iaq/pubs/insidestory.html>>
- [4] U.S. Energy Information Administration, "Summary Statistics for the United States, 1999-2010," Washington D.C., 2010, accessed by Web. on 13 Mar 2012, <http://205.254.135.7/electricity/annual>
- [5] McQuiston, F., Parker, J., and Spitler, F., 2005, *Heating, Ventilating, and Air Conditioning: Analysis and Design*, John Wiley and Sons.
- [6] Restivo, 1999, "A Turbulent Flow in Ventilated Rooms" PhD dissertation, University of London, U.K.
- [7] Betts, P.L. and Bokhari, I.H., 2000, "Experiments on Turbulent Natural Convection in an Enclosed Tall Cavity," *International Journal of Heat and Fluid Flow*, Vol. 21, pp. 675-683.
- [8] Blay, D., Mergui, S. and Niculae, C., 1992, "Confined Turbulent Mixed Convection in the Presence of a Horizontal Buoyant Wall Jet," in *Fundamentals of Mixed Convection*, ASME HTD, Vol. 213, pp. 65-72.
- [9] Jiang, Y. and Chen, Q., 2003, "Buoyancy-Driven Single-Sided Natural Ventilation in Buildings with Large Openings," *International Journal of Heat and Mass Transfer*, Vol. 46, pp. 973-988.
- [10] Basarir, M., 2009, "Numerical Study of the Airflow and Temperature Distributions in an Atrium," M.S thesis, Queen's University, Canada.
- [11] Horikiri, K., Yao, Y. and Yao, J., 2011, "Numerical Simulation of Convective Airflow in an Empty Room," *International Journal of Energy and Environment*, Vol. 5, pp. 574-581.
- [12] de Villiers, E., 2010, "Climate Control and HVAC Simulation for Occupied Spaces: Implementation and Validation," presented at the 5thOpenFOAM Workshop, Chalmers University, Gothenburg, Sweden, 21 Jun 2010.
- [13] Zuo, W. and Chen, Q., 2009, "Real Time or Faster-than-Real-Time Simulation of Airflow in Buildings," *Indoor Air*, Vol. 19, pp. 33-34.
- [14] Menter, F.R., Kuntz, M., and Langtry, R., 2003, "Ten Years of Industrial Experience with the SST Turbulence Model," *Turbulence, Heat and Mass Transfer*, Vol. 4.



**Alexander Kayne** received M.S in Mechanical Engineering from Washington University in St. Louis in 2011. His research interests include applications of heat transfer, thermodynamics and fluid mechanics to study the HVAC systems and energy efficiency of buildings by numerical simulations.  
E-mail address: [akayne@wustl.edu](mailto:akayne@wustl.edu)



**Ramesh K. Agarwal** received PhD in Aeronautical Sciences from Stanford University in 1975. His research interests are in the theory and applications of Computational Fluid Dynamics (CFD) to study the fluid flow problems in aerospace and renewable energy systems. He is currently the William Palm Professor of Engineering in department of Mechanical Engineering and Materials Science at Washington University in St. Louis, MO, USA. He is a Fellow of ASME, AIAA, IEEE, and SAE.  
E-mail address: [rka@wustl.edu](mailto:rka@wustl.edu)